CFSRC COLLOQUIUM

Proceedings of the Cold-Formed Steel Research Consortium Colloquium
20-22 October 2020 (cfsrc.org)

Appliance of plastic hinge method considering distortional buckling in pushover analysis of cold-formed rack structure

Yin, Lingfeng[1]; Shen, Xin[2]; Tang, Gan[3]; Li, Zhanjie[4]

Abstract

The objective of this paper is to develop a yielding surface of thin-walled cold-formed steel members subjected to distortional buckling, and then integrate the surface into pushover analysis of rack structures. Distortional buckling is one of the dominant buckling behaviors of rack members due to their intrinsic section profile. In this study, the Axial-Moment-Moment (PMM) interaction surface for a perforated omega column is established using the finite element method and compared with the theoretical one by EN 15512. It is found that the theoretical PMM domain might be conservative. Then, pushover analyses using these two PMM surfaces along with PMM from ASCE 7 are performed on a cold-formed steel rack. The pushover curve and failure mechanism of the models are analyzed with those from a detailed shell Finite Element model and a full-scale experiment. Finally, this approach of employing distortional PMM is comprehensively assessed from computational cost and reliability for its efficiency in engineering practice.

1. Introduction

Recently, the multi-layer rack structure made by cold-formed thin wall steel (CFTWS) has been widely used in logistics and warehousing fields. Nowadays, it is much more closely connected to our daily life, thus its security problem is of great importance.

1.1 Features of CFTWS

CFTWS is achieved by rolling or drawing steel belt or plate at room temperature, whose thickness is usually under 4 mm. Compared to hot-rolled steel section with the same area, CFTWS section has larger inertial radius and inertial moment. Additionally, CFTWS section has advantages in its high ratio of strength to weight, flexible shape and easy fabrication [1].

However, with ultra-thin plate and complex section shape to fully utilize its material strength, the stability or buckling of CFTWS members attracts prominent attention. At present, academia classifies the buckling of CFTWS members into three basis modes, which are global buckling, local buckling and distortional buckling respectively [2]. With regard to CFTWS open Ω-column which is commonly employed in rack structures, distortional buckling turns into the dominant factor in certain cases [3], and the buckling of members often behaves as a combination of two or three basis modes [4].

1.2 Analysis method of CFTWS members

After collecting massive test data of distortional buckling and local buckling from bending members with crimping C-shape and Z-shape sections, Schafer and Peköz established the direct strength method (DSM) for capacity calculation of CFTWS members [5]. Later, Schafer applied the data to the strength curve of distortional buckling which was put forward by Hancock et al. and then expanded the curve to local, distortional, global and their coupled buckling to analyze members' strength [6]. Therefore, DSM was further developed and improved.

Nevertheless, DSM provides strength formula of different buckling modes only for pure compressive or pure bending members. And the minimum result is chosen as a member's limit capacity, despite the buckling corresponding to that value never happens, which makes DSM conservative. For members under combined PMM load, AISI S100-12 [7] and EN 15512 [8] both give a linear equation of force interaction to estimate the limit capacity, which means a PMM domain like the surface of quadrangular pyramid. Bertocci et al.

[1] Yin, Lingfeng. Associate professor, School of Civil Engineering, Southeast University, Nanjing, China, eking@seu.edu.cn
[2] Shen, Xin. MA student, School of Civil Engineering, Southeast University, Nanjing, China, 220181084@seu.edu.cn
[3] Tang, Gan. Associate professor, Department of Civil Engineering, NUAA, Nanjing, China, tanggan@sina.com
[4] Li, Zhanjie. Associate professor, Department of Engineering, SUNY Polytechnic Institute, Utica, NY, USA, Zhanjie@sunypoly.edu

compared the PMM domain from large numbers of FEM simulations to that in EN 15512. Results indicated that the formula of EN 15512 has average 10% safety margin [9].

1.3 Analysis method of CFTWS structures

Mainstream methods for advanced structural analysis at present include plastic zone method and plastic hinge method [10].

Shell or solid element is adopted in plastic zone method to reflect the gradual development of plasticity. It is seen as an "accurate method" since it can consider most factors at present [11]. However, this method is too complex to analyze large scale structures, so it is mainly used to verify simplified method or experiment.

Plastic hinge method employs concentrated plastic hinge and beam-column element is chosen for analysis. It is assumed that the plastic hinge only exists at the end of each element. Therefore, this method cannot solve the development at a certain section or the distribution along the element of plastic hinge [12]. Due to the hypothesis above is not always true, and traditional beam-column element is unable to involve local and distortional buckling, the precision of plastic hinge method needs to be improved, although it has fast computational speed.

1.4 Work of this paper

In the previous pushover analysis of a shell FE model of 3-layer-3-span steel rack with 2 mm wall thick Ω-columns carried out by our group, the distortional buckling at the upper end of bottom layer columns is the main reason for the failure of structure [13].

However, it is complicated to build and calculate refined ABAQUS model with shell elements. For this reason, this paper wants to build FE model conveniently with beam-column element of SAP2000. In order to balance the computational price and precision, the PMM domain of plastic hinge is defined to reflect distortional buckling in line elements.

2. Two kinds of PMM domains

CFTWS open Ω-columns of N100 type with 2 mm wall thickness are chosen for analysis, as shown in Figure 1.

Relevant literature and analysis from CUFSM, a software of finite strip method, reveal that the buckling of N100 Ω-column with 700 mm length mainly comes from distortional buckling [14][15]. To achieve the PMM domain reflecting distortional buckling, 700 mm is selected as the length of members for FEM analysis and theoretical calculation.

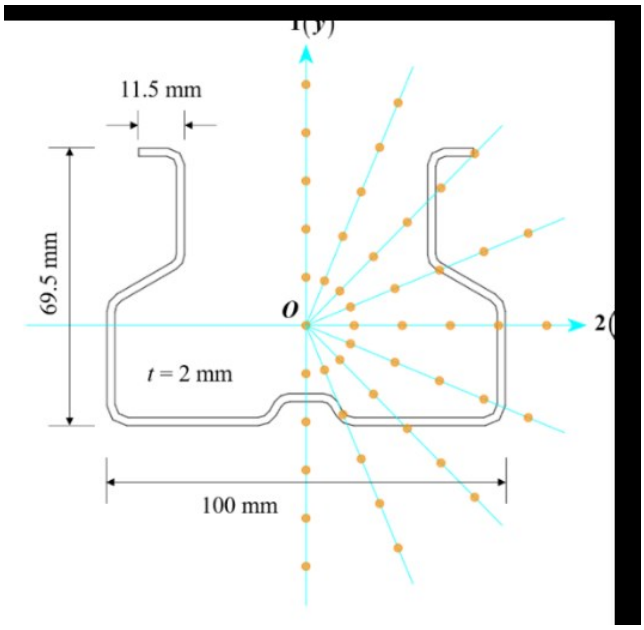

Figure 1: Section of N100 Ω-column and loading points

2.1 Numerical PMM domain by FEM

MATLAB is used to invoke ABAQUS to parametrically establish the shell FE model of N100 Ω-columns. Material property is defined as following: Young's modulus E = 210000 MPa, Poisson ratio v = 0.3, yield strength f_y = 263 MPa, ideal elastoplasticity. Two reference points (RP) are set at both ends of the column model, coupling all DOFs of the end section respectively. RP at supporting end is located at section centroid, whose translational DOFs are constrained. While the planar translational DOFs (U1, U2) and one rotational DOF (UR3) of the other RP at loading end are constrained. Displacement along the length of column is applied as loading approach.

At the beginning of analysis, first five modals are found by CUFSM, a certain combination of which is set as initial imperfection [16]. And then Riks analysis is operated in ABAQUS. By adjusting the location of RP at loading end, series of coordinate (P, M1, M2) as the column reaches limit capacity are obtained. The numerical PMM domain is finally formed by means of fitting these coordinates, where 1-aixs is the strong axis corresponding to y-axis and 2-axis is the weak axis corresponding to z-axis in EN 15512. Limited by the programing code, perforation is not included in this model. Because of the section symmetricity about 1-axis, the loading points are merely located on one side of 1-axis as shown in Figure 1.

It is found that in the results of FEM analysis:

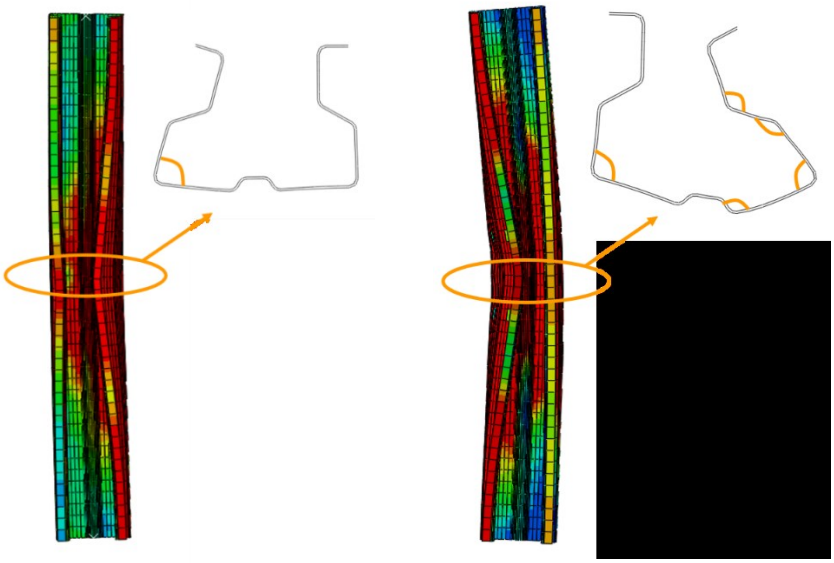

(a) Axial compression (b) Eccentricity towards strong axis

Figure 2: Distortional buckling of Ω-column by FEM

(1) When loading point is located at section centroid, distortional buckling is obvious, which makes up approximately 50% among three basis buckling modes, as shown in Figure 2(a).

(2) When loading point is eccentric towards strong axis, distortional buckling is quite obvious, as shown in Figure 2(b), which accounts for around 65%.

(3) When loading point is eccentric towards weak axis, and the web is under compression, the global buckling of web plate is prior to the distortional buckling of flanges. Therefore, in this case, global buckling takes main position and distortional buckling makes up less than 20%.

(4) When the web is under tension so as to no stable problem exists, as load eccentric towards weak axis rising, distortional buckling still happens first, which accounts for nearly 80%. This already can be seen as a "pure" distortional buckling.

What shall be pointed out is that the force on Ω-column is often eccentric towards strong axis in pushover. When M1 = M2 = 0, Ω-column is under axial compression and the ultimate axial force P is solved as 140344 N by ABAQUS.

2.2 Theoretical PMM domain by EN 15512

The limit capacity of bending and compressive members for which lateral-torsional buckling is a potential failure mode shall satisfy the following equation:

$$\frac{N_{\mathrm{Sd}}}{\chi_{\min} A_{\mathrm{eff}} f_{\mathrm{y}}} + \frac{k_{\mathrm{LT}} M_{\mathrm{y,Sd}}}{\chi_{\mathrm{LT}} W_{\mathrm{eff,y}} f_{\mathrm{y}}} + \frac{k_{\mathrm{z}} M_{\mathrm{z,Sd}}}{W_{\mathrm{eff,z}} f_{\mathrm{y}}} = 1 \qquad (1)$$

Where $\chi_{\min}=\min\{\chi_{\mathrm{db}}, \chi_{\mathrm{y}}, \chi_{\mathrm{z}}\}$, and χ is a reduction factor. Effective area of section A_{eff} is obtained according to the stub column compression test in A.2.1 of EN 15512 [8]**Error! Reference source not found.**. In Equation 1, χ_{db} reflects the influence from distortional buckling, while A_{eff} indicates a summary effect on the reduction of capacity by perforation and local buckling. In this paper, A_{eff} equals 426 mm^2 for N100 Ω-column with 2 mm wall thickness, while the gross area of section A_{g} equals 562 mm^2. Keeping the centerline of perforation consistent with that of the real member, apportion the lost area from A_{g} to A_{eff} to perforation area, and then the effective section is achieved as shown in Figure 3. It is adopted throughout the subsequent analysis.

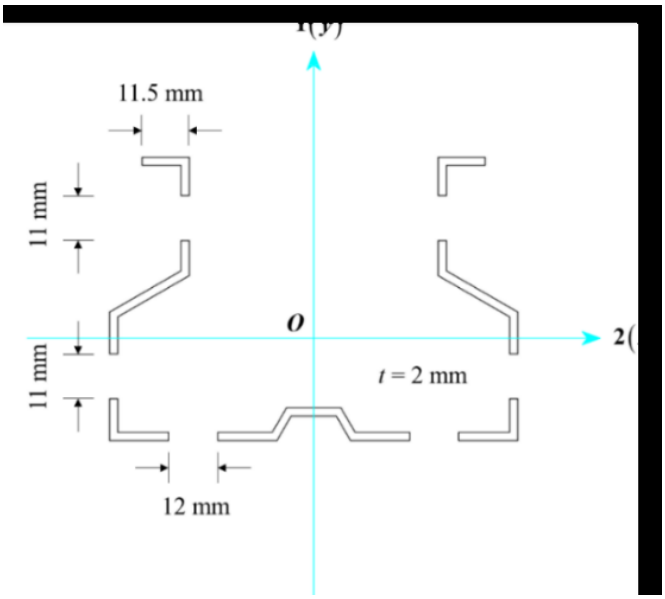

Figure 3: Effective section of N100 Ω-column

Parameters involving lateral-torsional buckling are calculated as follows:

$$\begin{cases} k_{\mathrm{LT}} = 1 - \dfrac{\mu_{\mathrm{LT}} N_{\mathrm{Sd}}}{\chi_z A_{\mathrm{eff}} f_{\mathrm{y}}}, \ \text{and } k_{\mathrm{LT}} \le 1 \\ \mu_{\mathrm{LT}} = 0.15\bar{\lambda}_z \beta_{\mathrm{M,LT}} - 0.15, \ \text{and } \mu_{\mathrm{LT}} \le 0.9 \\ \bar{\lambda}_z = \sqrt{\dfrac{A_{\mathrm{eff}} f_{\mathrm{y}}}{N_{\mathrm{z,cr}}}}, \ \beta_{\mathrm{M,LT}} = 1.1 \end{cases} \quad (80')$$

Where $N_{\mathrm{z,cr}}$ is the Eular critical load of ideal axial compressive member around its weak axis, and equivalent moment factor $\beta_{\mathrm{M,LT}}$ = 0.75 [17]. Since the length of column is just 700 mm, the slenderness ratio $\bar{\lambda}_z$ for flexural buckling is solved as 0.281, so as to make μ_{LT} a negative value. No matter what the design compression N_{Sd} is, k_{LT} always equals 1.

With regard to CFTWS section, we have:

$$\begin{cases} \chi_{\mathrm{LT}} = \dfrac{1}{\Phi_{\mathrm{LT}} + \sqrt{\Phi_{\mathrm{LT}}^2 - 0.75\bar{\lambda}_{\mathrm{LT}}^2}}, \ \text{and } \chi_{\mathrm{LT}} \le 1 \\ \Phi_{\mathrm{LT}} = 0.5\left[1 + 0.34\left(\bar{\lambda}_{\mathrm{LT}} - 0.4\right) + 0.75\bar{\lambda}_{\mathrm{LT}}^2\right] \\ \bar{\lambda}_{\mathrm{LT}} = \sqrt{\dfrac{W_{\mathrm{y}} f_{\mathrm{y}}}{M_{\mathrm{cr}}}} \end{cases} \quad (81')$$

Where M_{cr} is member's critical moment of elastic bending-torsional buckling under pure bending state. It is solved that $\bar{\lambda}_{\mathrm{LT}}$= 0.224 and Φ_{LT} = 0.489, so χ_{LT} equals 1. Then Equation 1 can be simplified as below:

$$\frac{N_{\mathrm{Sd}}}{\chi_{\min} A_{\mathrm{eff}} f_{\mathrm{y}}} + \frac{M_{\mathrm{y,Sd}}}{W_{\mathrm{eff,y}} f_{\mathrm{y}}} + \frac{k_z M_{\mathrm{z,Sd}}}{W_{\mathrm{eff,z}} f_{\mathrm{y}}} = 1 \quad (82')$$

The formula to calculate k_z is similar to that for k_{LT}. Just substitute μ_{LT} for μ_z, but k_z shall not exceed 1.5. For the column in this paper, as compression decreases, k_z descends from 1.5 to 1.0, therefore it can be seen as an enlargement of moment around the weak axis.

Let $P_{\mathrm{y}} = \chi_{\min} A_{\mathrm{eff}} f_{\mathrm{y}}$, $M_{\mathrm{y1}} = W_{\mathrm{eff,y}} f_{\mathrm{y}}$, $M_{\mathrm{y2}} = W_{\mathrm{eff,z}} f_{\mathrm{y}}$, Equation 4 can be transformed into below:

$$\frac{P}{P_{\mathrm{y}}} + \frac{M_1}{M_{\mathrm{y1}}} + \frac{k_2 M_2}{M_{\mathrm{y2}}} = 1 \quad (83')$$

This is the final expression given by EN 15512 of PMM domain at limit capacity for columns in this paper. In the case of M_1 = M_2 = 0, Ω-column is under axial compression and P=$\chi_{\min} A_{\mathrm{eff}} f_{\mathrm{y}}$ =108750 N. While M_2 =0, the combination of P and M_1 will cause the edge fiber of one side flange to reach material yield strength, which is the upper limit of theoretical design strength. While M_1 = 0, Equation 5 enlarges the moment around weak axis, which is a safer handling. But from the point of section shape, even though the web plate has reached yield strength, there still exist two flanges, which make up the most area of section, to bear the load. Furthermore, two flanges are an effective constraint to the yielded web plate. This explanation is consistent with the view of Lorenzo Bertocci et al. in literature [9] "From the observation of both experimental and numerical curves, the failure of uprights always occurs when large parts of the specimen are yielded."

2.3 Comparison between two PMM domains

To solve the defect that the numerical PMM domain by ABAQUS does not include perforation while the theoretical one by EN 15512 does, a scale factor *c* = 108750/140344 = 0.775 is introduced referring to literature [9]**Error! Reference source not found.**. All numerical results are multiplied by *c* as a rough way to consider perforation, and then the modified coordinates (P, M_1, M_2) are received.

P_{y}, M_{y1} and M_{y2} are used to normalize two groups of coordinates by ABAQUS and EN 15512 respectively, then two PMM domains of limit capacity for Ω-columns are plotted in one coordinate system as shown in Figure 4.

It is found that the numerical PMM domain is always convex and can totally wrap the theoretical one. As M_1 takes the maximum absolute value, M_2 does not equal zero, which means there is some kind coupling relationship between them. The distinction between two PMM domains is especially obvious when M_2 takes negative value, meaning the web plate is in tension. In this case the buckling mode for member is almost pure distortional buckling, while global buckling takes main position as M_2 is positive. These features are similar to that in B. G. Wang's master thesis,

where a numerical PMM domain for N90 Ω-column is plotted [18].

Lorenzo Bertocci et al. reveals that the numerical PMM domain is not symmetric about M_2, because tension failure is usually determined by material yield strength, while compression failure is determined by stability [9]. However, EN 15512 does not include this consideration so as to present a biaxial symmetric PMM domain. It is also found that when $P = 0.5P_y$, the maximum value of $|M_2|/M_{2y}$ has exceeds 1. When $P = 0.2P_y$, so does it for $|M_1|/M_{1y}$. This means the limit capacity for CFTWS Ω-column, if post-buckling strength is fully utilized, can surpass the yield strength of edge fiber. But current criteria are too conservative to make use of it.

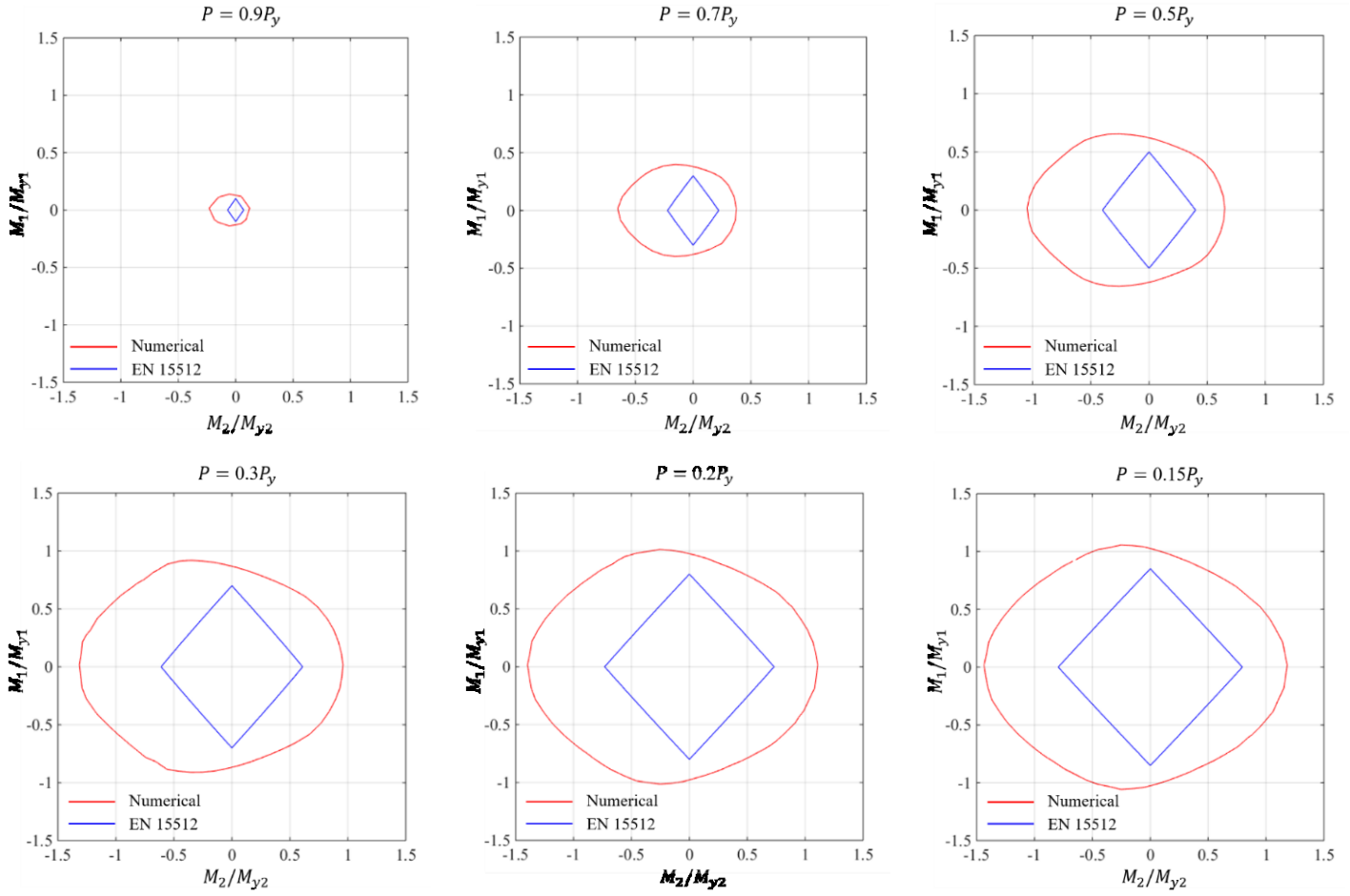

Figure 4: Comparison between two normalized PMM domains from section view

3. Pushover analysis

According to plastic hinge method, PMM hinges are set on columns where the relative distance from the end is 0.05, and M hinges are set on beams at the same position, based on the original frame model. The yield moment and rotation of M hinge are defined by equivalent stiffness method combined with the hysteretic curve of previous connection test by our group [19].

In order to include perforation in frame model, two schemes are tried: (i) the effective section in Figure 3 and the numerical PMM domain without multiplying c are used. (ii) the gross section in Figure 1 and the numerical PMM domain multiplied by c are used. Results indicate that scheme (i) is more suitable.

From previous research, it is known that the performance of plastic hinge is extremely affected by axial compression ratio. So that two representative cases are analyzed next.

3.1 Model with 2 mm wall thickness

It is simply estimated that the axial compression ratio of bottom rack column with 2 mm wall thickness is larger than 0.2. The pushover curves of base shear and displacement with different PMM domains adopted in plastic hinge are illustrated in Figure 5. As PMM domain represents the performance when members reach limit capacity, three curves from SAP2000 are nearly coincide at the beginning. Compared to the curve from ABAQUS, they all reflect the features of equivalent stiffness method.

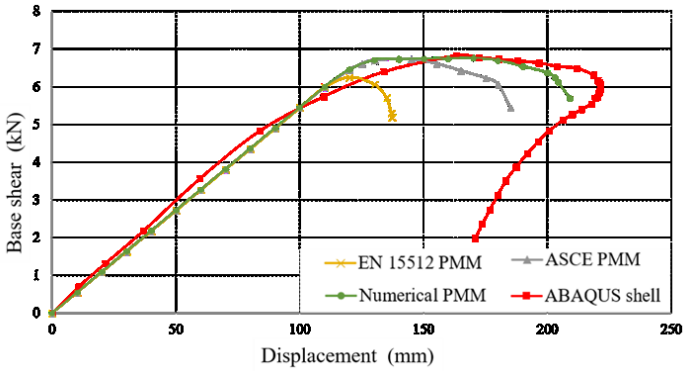

Figure 5: Pushover curves of FE models (t = 2 mm)

Among three curves from SAP2000, model with EN 15512 PMM domain has lowest limit capacity and ductility. Model with ASCE PMM domain, which is prepared by SAP2000 for hot-rolled section, shares almost the same limit capacity with numerical model in this paper, but the latter has better post-buckling performance and is the most closed to ABAQUS curve. This phenomenon also proves the conservation of PMM domain defined by EN 15512.

As to the ultimate state of structure in Figure 6, there all exist E level plastic hinges at upper end of bottom column, which means a “soft layer failure” mechanism [20]. This is similar to that of ABAQUS shell model as shown in Figure 7. It can be clearly observed that large area enters plasticity at upper end of bottom column and obvious distortional buckling happens. What differs is that EN 15512 model announces structural failure not until plastic hinge on beams widely occurs, which should be avoided in design.

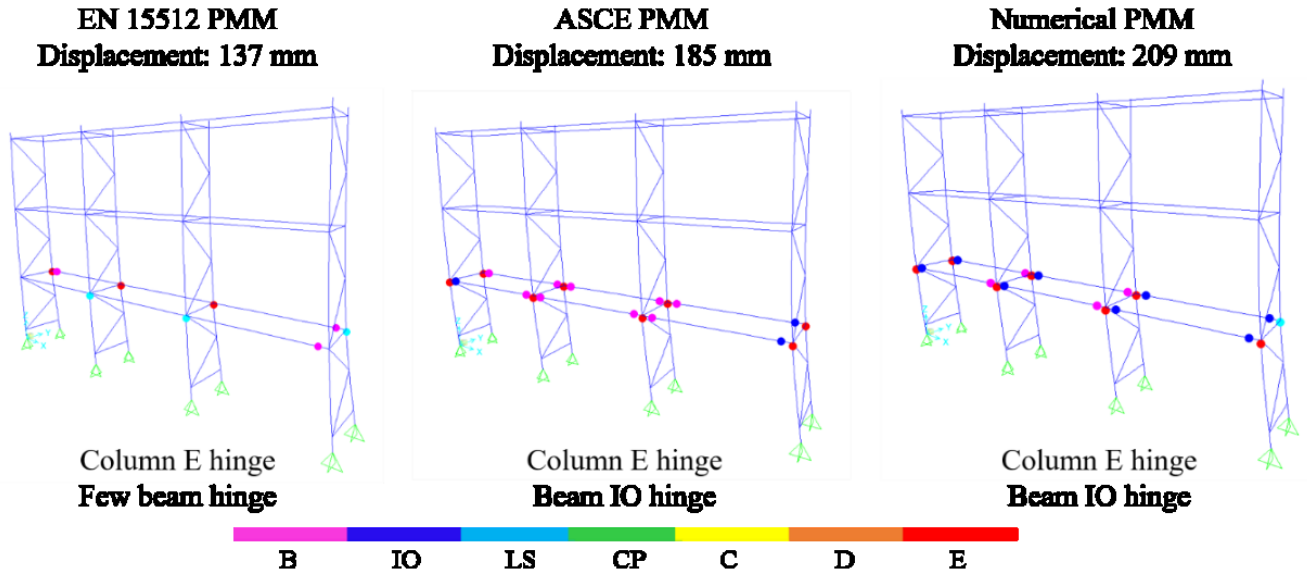

Figure 6: Ultimate state of SAP2000 model (t = 2 mm)

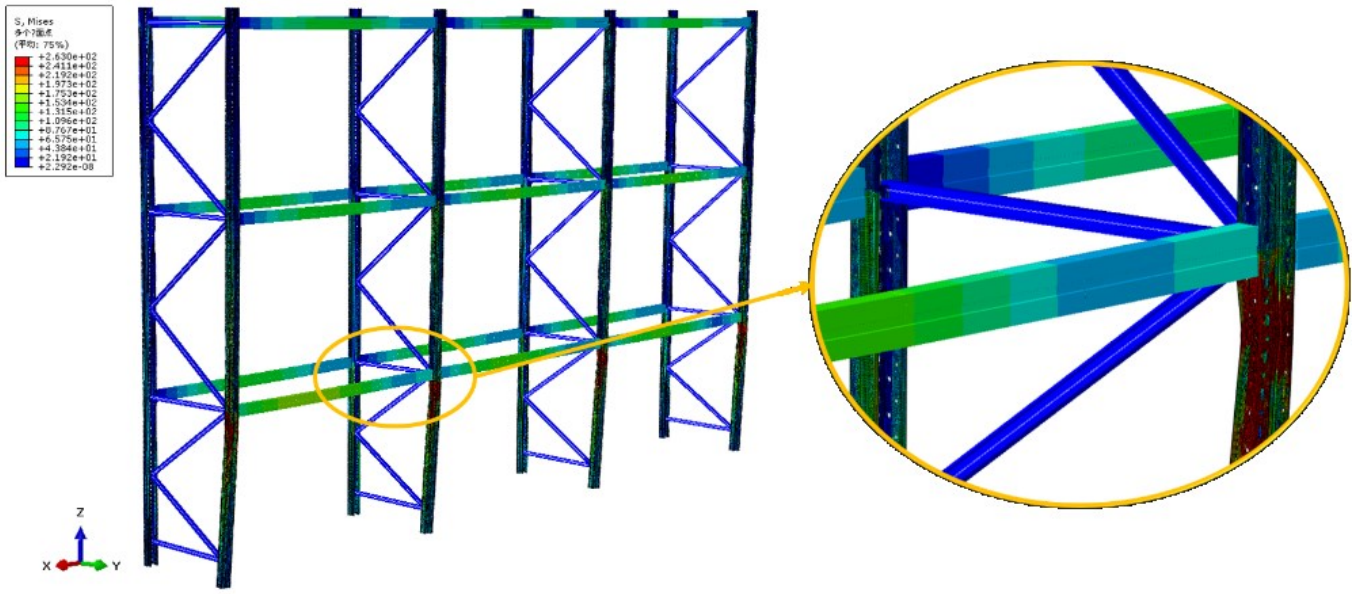

Figure 7: Ultimate state of ABAQUS model (t = 2 mm)

3.2 Model with 3 mm wall thickness

After wall thickness is added to 3 mm, which is consistent with the rack in experiment, columns' axial compression ratio is much smaller than 0.2. The theoretical and numerical PMM domains in this part are recalculated according to methods in 2.1 and 2.2 respectively.

It is illustrated in Figure 8 the early stiffness of three SAP2000 frame models approaches to that of experiment, while their later stiffness is similar to that of ABAQUS shell model. Curves of ASCE and numerical models almost coincide. Possible explanation is when section thickened, its property gradually transfers from thin-walled section to hot-rolled section, and there is still no rule to precisely define their circumscription. Therefore, the ASCE PMM domain possesses applicability to some degree.

Similarly, ultimate state is selected to analyze the failure mechanism of structure as shown in Figure 9. It is found that EN 15512 model comes to soft layer failure as lateral displacement just reaches 180 mm. The plastic development and failure mechanism between ASCE and numerical models are proximate. In order to observe plastic hinges, the ultimate lateral displacement of these two models both chooses 250 mm. Their failure mechanism is predicted to be global failure caused by plastic hinges at two ends of beams [20]. Therefore, these two models have outstanding ductility and there is still a quite extension in curves after the chosen ultimate lateral displacement. What differs is that absolutely no plastic hinge occurs on column in ASCE model in pushover process, while IO plastic hinges finally occur at upper end of bottom middle columns in numerical model. This can also explain why the curves of ASCE and numerical models coincide, as the combined load still has a long way to reach the surface of ASCE and numerical PMM domains.

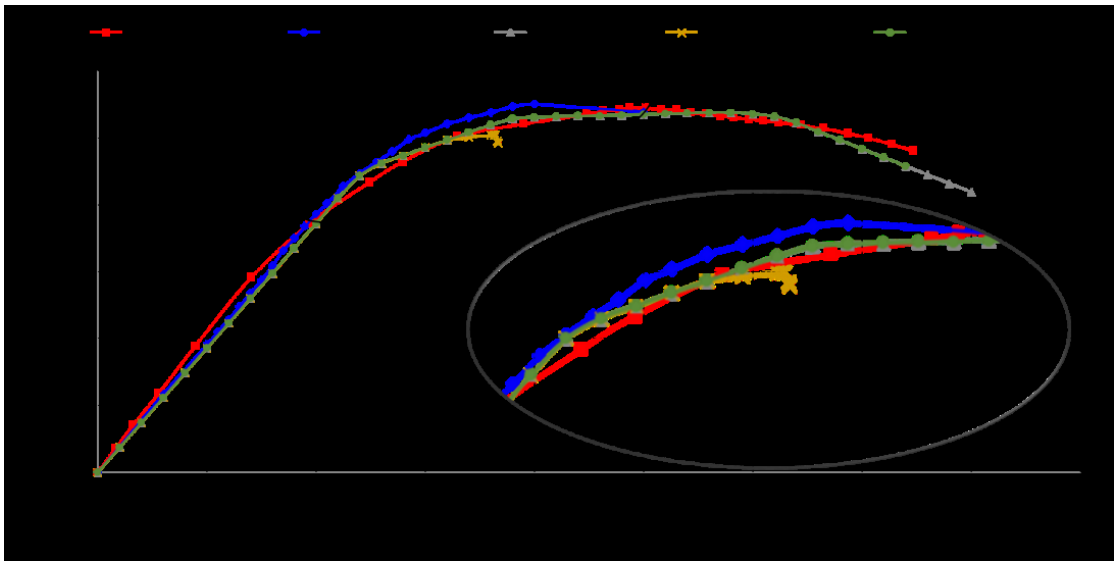

Figure 8: Pushover curves of FE models (t = 3 mm)

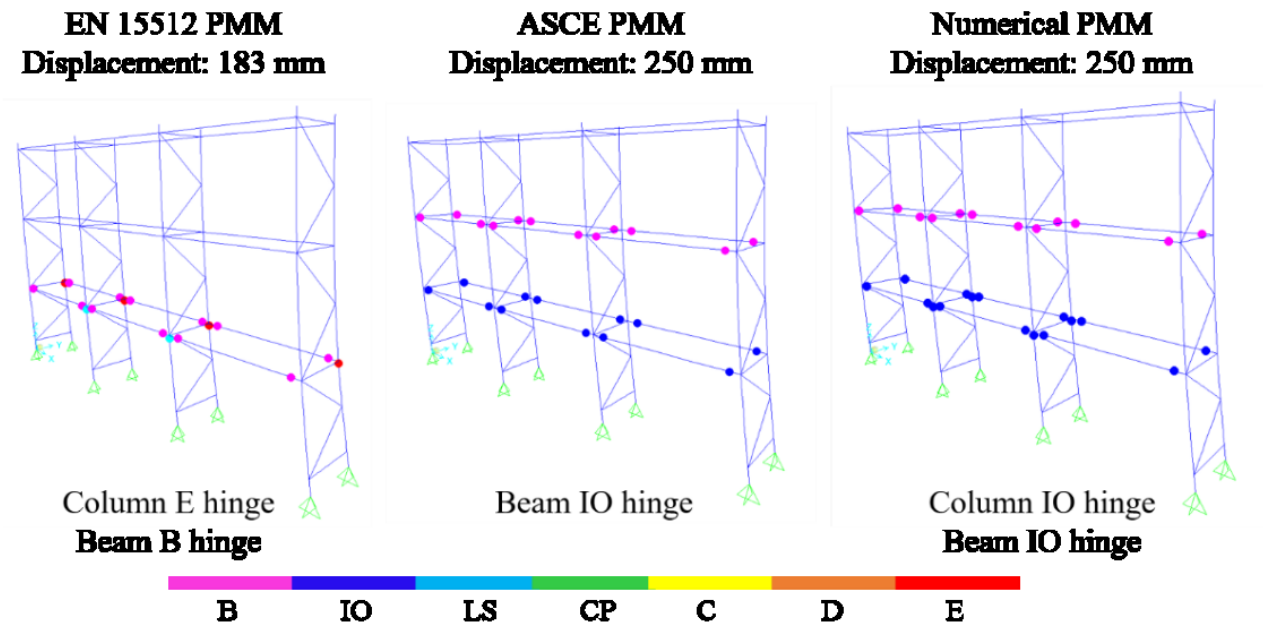

Figure 9: Ultimate state of SAP2000 model (t = 3 mm)

The state of ABAQUS shell model as lateral displacement reaches 250 mm is shown in Figure 10. There is no obvious buckling in structure but separated areas around perforation at upper end of bottom column enter plasticity. So that it can be assessed that the numerical model is more closed to ABAQUS model in failure mechanism.

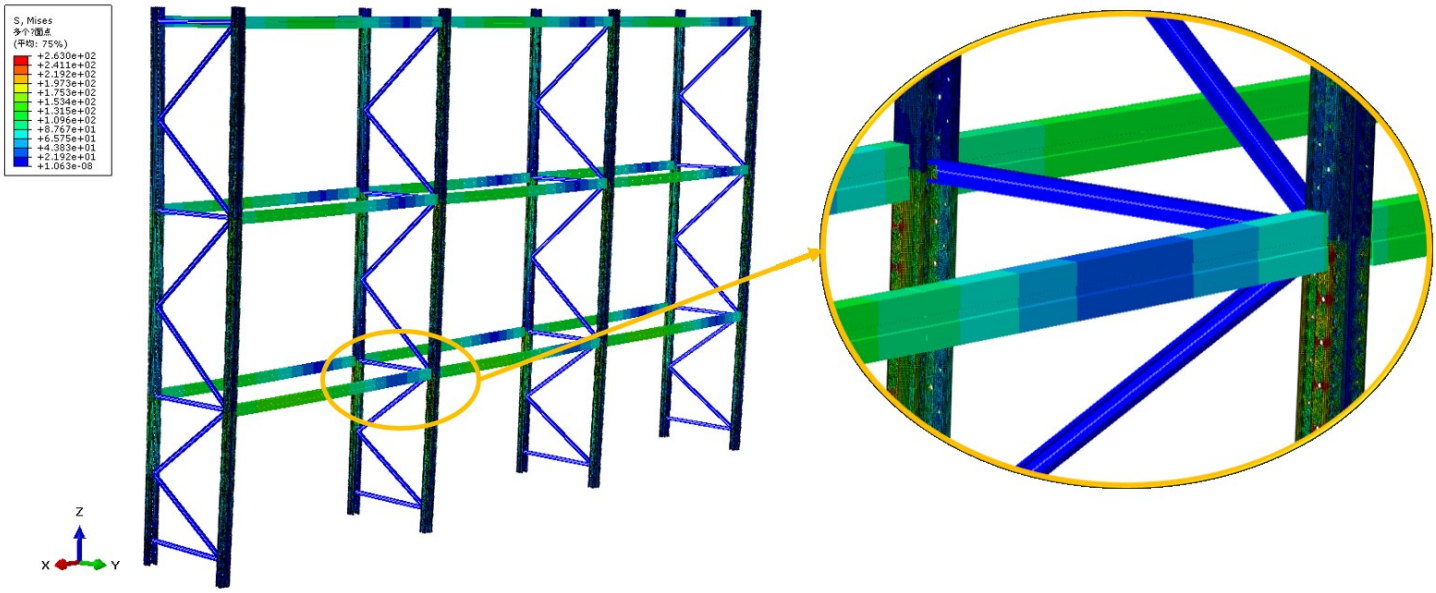

Figure 10: Ultimate state of ABAQUS model (t = 3 mm)

4. Conclusion

With regard to 700 mm long, CFTWS N100 perforated Ω-column, this paper compares the theoretical PMM domain defined by EN 15512 and the numerical one calculated by FEM, both of which involve distortional buckling. It reveals that PMM domain from EN 15512 is too conservative, especially under eccentric load towards the weak axis of section meanwhile the web plate is in tension.

This paper also provides a scheme to consider perforation in beam-column element, i.e., keeping the centerline of perforation consistent with that in real member, apportion the shrinking area from gross section to effective section to perforation area. This scheme is proved to be successful in subsequent analysis.

Furthermore, this paper improves the plastic hinge method by inserting three different PMM domains (EN 15512 PMM, numerical PMM and ASCE PMM which is originally provided by SAP2000) into plastic hinge to introduce distortional buckling. The pushover curve and failure mechanism of different models are compared. It is found that the pushover curve of frame model with numerical PMM domain is the most closed to that of shell model, and they share the same failure mechanism. This indicates it is feasible to introduce the influence of distortional buckling with PMM domain inserted into plastic hinges. Using this method to replace shell model can greatly raise analysis efficiency in large scale engineering practice.
Additionally, with wall thickness of section added from 2 mm to 3 mm, the ASCE PMM formula for hot-rolled steel section actually possesses certain applicability to pushover analysis of rack models in this paper. However, the applicable criterion is still to be researched further.

5. Acknowledgments

We are grateful to Natural Science Foundation of Jiangsu Province for their financial support (No: BK20191268) to this paper.

References

[1] B. Janarthanan, M. Mahendran, and S. Gunalan. Numerical modelling of web crippling failures in cold-formed steel unlipped channel sections. J. Constr. Steel Res., 2019, 158: 486-501.
[2] B. Schafer. Review: The direct strength method of cold-formed steel member design. J. Constr. Steel Res., 2008, 64: 766–778.
[3] L. Yin, Z. Xu, H. Huang, et al. Analysis of axial bearing capacity of three times cold-formed thin-walled lipped channel column with holes. JCAEE, 2013, 35(3): 81-87.
[4] S. Chen. Local interactive buckling and distortional buckling of lipped channels. J. Building Struct., 2002, 23(1): 27-31.
[5] B. Schafer, and T. Peköz. Direct strength predication of cold-formed steel members using numerical elastic buckling solutions. Thin-Walled Struct., 1998: 137-144.
[6] B. Schafer. Local, distortional and Euler buckling of thin-walled columns. J. Struct. Eng., 2002, 128(3): 289-299.
[7] AISI S100-12, North American Specification for the Design of Cold-Formed Steel Structural Members. Washington D.C., U.S.A.: AISI, 2016.

[8] EN 15512, Steel static storage systems – Adjustable pallet racking systems – Principles for structural design. Brussels, Belgium: CEN, 2009.
[9] L. Bertocci, D. Comparini, G. Lavacchini, et al. Experimental, numerical, and regulatory P-Mx-My domains for cold-formed perforated steel uprights of pallet-racks. Thin-Walled Struct., 2017, 119: 151-165.
[10] Liew, J. Richard, D. White, et al. Second-order refined plastic-hinge analysis for frame design, Part I. J. Struct. Eng., 1993, 119(11): 3196-3216.
[11] Z. Wang. Advanced analysis of multi-segments element for steel structures. Thesis for PhD. degree, Nanjing: Southeast University, 2006.
[12] K. Zhou, Q. Song, and J. Jia. Advanced analysis for practical steel frame design. Proc. Steel Building Struct., 2002, 4(2): 33-38.
[13] L. Yin, G. Tang, and Z. Li. Computational modeling of thin-walled cold-formed steel pallet rack structures. Proceedings of the 8th International Conference on Thin-walled Structures, 2018.
[14] A. Crisan, V. Ungureanu, and D. Dubina. Behaviour of cold-formed steel perforated sections in compression. Part 1 – Experimental investigations. Thin-Walled Struct., 2012, 61: 86-96.
[15] A. Crisan, V. Ungureanu, and D. Dubina. Behaviour of cold-formed steel perforated sections in compression. Part 2 – Numerical investigations and design considerations. Thin-Walled Struct., 2012, 61: 97-105.
[16] M. Pastor, M. Casafont, J. Bonada, et al. Imperfection amplitudes for nonlinear analysis of open thin-walled steel cross-sections used in rack column uprights. Thin-Walled Struct., 2014, 76: 28-41.
[17] EN 1993-1-3, Design of steel structures – General rules – Supplementary rules for cold-formed members and sheeting. Brussels, Belgium: CEN, 2006.
[18] B. Wang, Experimental research and analysis on beam-to-column connectors in assembled steel racks under low-cycle reversed and fatigue loading. Thesis for MA. degree, Nanjing: Southeast University, 2013.
[19] Z. Zheng, Research on new type removable beam-upright connections of high ductility in storage structures under low-cycle reversed loading. Thesis for MA. degree, Nanjing: Southeast University, 2015.
[20] A. Kanyilmaz, C. Castiglioni, G. Brambilla, et al. Experimental assessment of the seismic behavior of unbraced steel storage pallet racks. Thin-Walled Struct., 2016, 108: 391-405.
[21] M. Zhang, Performance based seismic analysis and experimental research of dense frame-truss storage structure. Thesis for MA. degree, Nanjing: Southeast University, 2015.